Characterization of Large-Scale Structures in a Forced Ducted Flow with Dump

K. C. Schadow* and K. J. Wilson†
Naval Weapons Center, China Lake, California
and
E. Gutmark‡
Tel Aviv University, Tel Aviv, Israel

A forced, subsonic ducted airflow with a dump was studied using hot-wire anemometry. The flow was forced by exciting the duct resonant acoustics. Flow structures (vortices) with high azimuthal coherence and high spatial and temporal periodicity were generated in the shear flow at the dump when the forcing frequency matched the first subharmonic of the initial vortex shedding frequency or the preferred mode frequency. By forcing the flow at the preferred mode frequency, mixing was enhanced in the shear and pipe flow regimes. A visual description of the coherent structures was obtained in water flow tests.

Nomenclature

A_p = relative pressure amplitude
CL = centerline
D = diameter of inlet duct (jet exit)
$D_{t,CH}$ = throat diameter of acoustic cavity (chamber)
$D_{t,RV}$ = throat diameter of rotating valve
E_V = energy of velocity fluctuation
f_F = forcing frequency (frequency of rotating valve)
f_i = initial vortex shedding frequency
f_j = preferred mode (jet column) frequency
f_{1L} = frequency of first longitudinal acoustic mode
f_{1M} = first vortex merging frequency
f_{2L} = frequency of second longitudinal acoustic mode
L_{CH} = chamber length measured from dump
P = mean chamber pressure
R = radial coordinate
Re = Reynolds number
$R_{\max}$ = maximum cross-correlation coefficient
R_0 = cross-correlation coefficient at $\tau = 0$
$R_{U/U_0=0.5}$ = jet width at which U has decreased to 50% of the maximum velocity
$R_{1,2}$ = cross-correlation coefficient
$S.L.$ = shear layer
St_i = Strouhal number based on f_i
St_j = Strouhal number based on f_j
U = local mean velocity
U_0 = jet exit velocity at dump
u' = axial velocity fluctuation intensity
X_{HW} = axial hot-wire position from dump
X_{HW1} = axial position of first of two hot wires
α = angle between two hot wires
α_{HW1} = azimuthal position of first of two hot wires
$(\Delta p)_{rms}$ = rms value of pressure fluctuation amplitude
ΔX = axial distance between two hot wires
θ = momentum thickness, $\theta = \int_0^{R_{\text{cutoff}}} \frac{U}{U_0}\left(1 - \frac{U}{U_0}\right) dR$
θ_0 = initial momentum thickness of shear layer
τ = time
ν = kinematic viscosity

Received Nov. 18, 1985; revision received Jan. 15, 1987.

*Supervisory General Engineer.
†Aerospace Engineer.
‡Research Scientist; currently at the Naval Weapons Center, China Lake, CA.

Introduction

THE role of the shear layer's large-scale turbulent structures in mixing processes and jet noise generation has been studied over the past 10 years.[1-4] Recent attention has been given to a structure's potential as a driver of combustion-induced pressure oscillations.[5-7] In this context, the interaction between the large-scale turbulent structures and the acoustic waves excited in the combustor cavity is of special interest. In addition, the control of these structures for mixing enhancement purposes is of high practical importance.

The effect of acoustic excitation on large-scale flow structures has been primarily studied in freejets[8,9]; however, little is known about the acoustics/shear layer interaction in ducted flows, especially at high Reynolds numbers and initial turbulent conditions. This paper deals with a subsonic, ducted airflow with a dump discharged into a chamber that can behave as an acoustic cavity. Specifically, nonreacting tests were made to study the interaction between the acoustic waves and the different stages of the shear layer development that will be described in this paper.

It is generally known that a shear layer, originating from the inlet duct at the jet exit, develops (as a result of background perturbations) instability waves that roll up into coherent structures. The roll-up of these axisymmetric vortices occurs at the most amplified frequency or the initial vortex shedding frequency f_i. This frequency, when scaled with the initial shear layer momentum thickness θ_0 and the jet exit velocity U_0 yields a Strouhal number of $St_i = f_i \cdot \theta_0 / U_0$ that is predicted to be $St_i \simeq 0.017$ by linear instability theory.[10]

The initially shed vortices merge as they are convected downstream.[11-13] Due to merging, the shear layer spreads and the passage frequency of the vortices in the shear layer drops. In laminar flow, the passage frequency after the first vortex merging, called the first vortex merging frequency f_{1M}, is the first subharmonic of f_i.

The energy level of the flow instability frequencies f_i and f_{1M} varies in the streamwise direction.[14] Near the axial position where the initial vortex roll-up occurs, f_i reaches its saturation level, while f_{1M} reaches the highest energy where the first vortex merging occurs. Additional vortex mergings can occur before the jet reaches the end of the potential core.

The velocity fluctuations at the end of the potential core were observed to have a characteristic frequency called the jet column or preferred mode frequency f_j. When this frequency is scaled with the jet exit diameter D and U_0, it yields a Strouhal number of $St_j = f_j \cdot D/U_0$. The range of St_j was found in a previous investigation to be between 0.25 and 0.5.[15]

Based on this description of the shear layer development, the objectives of the nonreacting tests can be defined as follows:

1) To determine the unforced shear layer instability frequency f_i, the subsequent merging frequencies, and the preferred mode frequency f_j of freejets and ducted jets and to identify the large-scale, coherent structures related to these instabilities.

2) To determine the jet flow response to acoustic waves, especially when the forcing frequency matches the unforced shear layer instability frequencies.

3) To characterize the axial and azimuthal development of the coherent structures under forcing conditions using hot-wire anemometry and flow visualization techniques.

4) To determine the effect of the coherent structures on mixing both in the shear layer and pipe flow regimes when forcing was applied at the preferred mode frequency.

Experimental Setup

Two test setups were used, one with airflow using hot-wire anemometry and the other with water flow for flow visualization. The schematic of the experimental setup with airflow is shown in Fig. 1. A jet from a duct having a diameter of $D = 6.35$ cm was injected into a chamber with variable length L_{CH}, diameter $2D$, and throat area corresponding to $D^2_{t,CH} = 0.256D^2$. In some of the experiments, only section A of the setup was used, giving a freejet emanating from a pipe. Most measurements were done using the entire system both with and without forcing. The airflow velocity in the inlet duct varied from $U_0 = 50$–140 m/s, corresponding to a maximum Reynolds number of $Re = U_0 D/\nu = 7 \times 10^5$. In this entire velocity range, the mean velocity profile at the jet exit was that of a fully developed turbulent pipe flow with a turbulence intensity of 13% at the nozzle's center. The majority of the ducted-flow tests were performed at $U_0 = 50$ m/s, which corresponds to $Re = 4.5 \times 10^5$ at $P = 186$ kPa.

In the tests with forced acoustics, the forcing amplitude was varied by changing the throat diameter of the rotating valve $D_{t,RV}$, relative to the throat diameter of the acoustic cavity $D_{t,CH}$. Four forcing amplitudes corresponding to $D^2_{t,RV}/D^2_{t,CH} = 0.09$, 0.18, 0.27, and 0.51 were applied at three nominal forcing frequencies of $f_F = 230$, 300, and 460 Hz. Each f_F was tuned to match the first longitudinal mode frequency, f_{1L}, of the chamber determined by the velocity of sound in the chamber and the chamber length L_{CH}, measured between the dump and nozzle. For $f_F = 460$ Hz, a second chamber length was used to match f_F with the second longitudinal mode frequency f_{2L} of the chamber. In these tests, proper matching between f_F and f_{1L} (or f_{2L}) was obtained by adjusting f_F during each test to a frequency at which the highest pressure amplitudes were achieved as determined by online pressure frequency analysis. Depending on f_F and $D^2_{t,RV}/D^2_{t,CH}$, the rms value of the pressure fluctuation amplitude $(\Delta p)_{\text{rms}}$ varied between 0.05 and 1.7% of the mean chamber pressure P. For the pressure amplitude measurements, the pressure transducer (piezoquartz Kistler transducer) was located near the dump at $L_{CH} = 0.4\ D$.

Table 1 summarizes the test conditions with L_{CH}/D, f_F, $D^2_{t,RV}/D^2_{t,CH}$, and $(\Delta p)_{\text{rms}}$ normalized by P. Hot-wire anemometry was used to determine the velocity fluctuation properties, mean velocities, and turbulence.

For the velocity fluctuation measurements, one hot wire was used to determine the velocity spectra in the shear flow at the dump and two hot wires to determine the temporal and spatial cross correlations in the shear and pipe flow regimes of the chamber. For the mean velocity and turbulence measurements, the single hot-wire probe was mounted on a high-precision, computer-controlled traverse mechanism. The calibration, data acquisition, and data reduction were done on a VAX 11/750 computer. The analog output from the hot-wire anemometer was digitized at 1 kHz for approximately 1 s to obtain 940 samples at each radial position. The mean and fluctuation values were then determined from these 940 samples. Measurements were made at 2.54 mm increments in the radial direction, except at the dump where a 0.8 mm resolution was required. High inaccuracies in the measurements were expected in the recirculation zone due to flow reversal; therefore, measurements were done only up to the edge of the jet, near the dump plane.

The water-tunnel model for the ducted jet with dump had the same geometric dimensions as the setup for the airflow tests. The jet exit velocity was $U_0 = 0.5$ m/s, which corresponded to a Reynolds number of $Re = 3 \times 10^4$ based on D. The initial vortex shedding frequency was estimated to be about $f_i = 10$ Hz based on a Strouhal number of

$$St_i = (f_i \cdot \theta_0)/U_0 = 0.02$$

from the airflow tests. The boundary-layer momentum thickness θ_0 at the jet exit was estimated using standard boundary-layer equations. The preferred mode frequency was estimated to be about $f_j = 2.5$ Hz, based on a preferred mode Strouhal number of

$$St_j = (f_j \cdot D)/U_0 = 0.3$$

from the airflow tests.

The flow was excited by using a rotating butterfly valve in the inlet duct. The velocity fluctuation amplitude was 3% of the mean velocity; the excitation frequencies tested were $f_F = 5$ Hz (or the first subharmonic of f_i) and $f_F = 2.5$ Hz (or the preferred mode frequency). The flow was visualized by injecting colored water into the shear layer at the dump and illuminating the flow with a slot lamp.

Results and Discussion

Shear Layer Structure

The measurements of the free and ducted air jet velocity fluctuation spectra, in addition to the flow visualization in

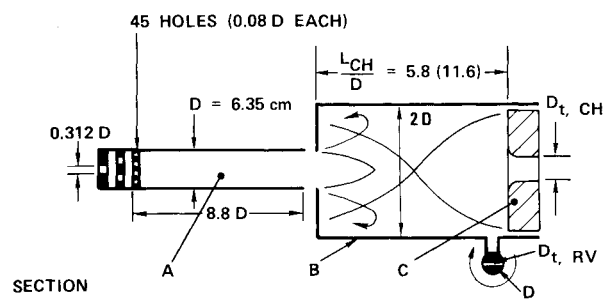

Fig. 1 Test setup (airflow).

the ducted water facility, were used to study the role of the large-scale structures in this flow. The frequency content of the velocity fluctuations was determined from spectral analysis along the shear layer for $0<X_{HW}/D<4.4$. The spectral measurements were done at different radial positions across the shear layer, but only the spectral distribution at the jet half-width ($R_{U/U_0=0.5}$) are presented in the paper. At the center of the jet nozzle (dump plane) ($X_{HW}/D=0$), the jet exhibited a typical turbulent spectrum without any distinct peaks.[16]

A typical spectrum of the velocity fluctuation on the shear layer center of the freejet at $X_{HW}/D=0.4$ is shown in Fig. 2. Three distinct peaks at $f=684$, 411, and 215 Hz were identified. The energy level of these peaks is determined by both the upstream initial disturbances emerging from the jet nozzle,[15,17] and the specific amplification characteristics of the jet shear layer. In a nondiverging parallel shear layer, the most amplified frequency can be predicted by the linear instability theory[7] ($St=0.017$). In a diverging shear layer, the shear layer thickness increases downstream and the growth rate of each frequency component is changing in the downstream direction according to the local Strouhal number. The energy level of each component at a specific axial location is thus determined not only by the local growth rate but also by its history of growing. The highest frequency (684 Hz), when scaled with θ_0 and U_0, yielded the Strouhal number $St=(f\cdot\theta_0)/U_0=0.0178$. This value is predicted by the linear instability theory to be the most amplified frequency in the initial shear layer. Therefore, this frequency (684 Hz) was identified as the initial vortex shedding frequency f_i.

The second peak (411 Hz) was dominant in the spectrum measured at this location and remained dominant up to a distance of $X_{HW}/D=1.5$, where the higher frequency peak has completely disappeared. At this axial location, the local Strouhal number equals 0.035, which is close to the neutral Strouhal number. As a result, the frequency is attenuated farther downstream. The spectrum shown in Fig. 2 represents the relative energy level across most of the shear layer width at this location.

The third peak (215 Hz) was dominant in the spectrum at $X_{HW}/D=2.8$ on the centerline (Fig. 3). When this frequency was scaled with D and U_0, it yielded the Strouhal number $St=(f_j\cdot D)/U_0=0.269$, which is within the range of the preferred mode Strouhal number found in previous investigations.[15] Therefore, the third-peak frequency (215 Hz) was identified as the preferred mode frequency f_j. From the previous considerations, it is clear that the peaks in Fig. 2 can be identified as traces of large-scale flow structures as they evolve in the jet shear layer.

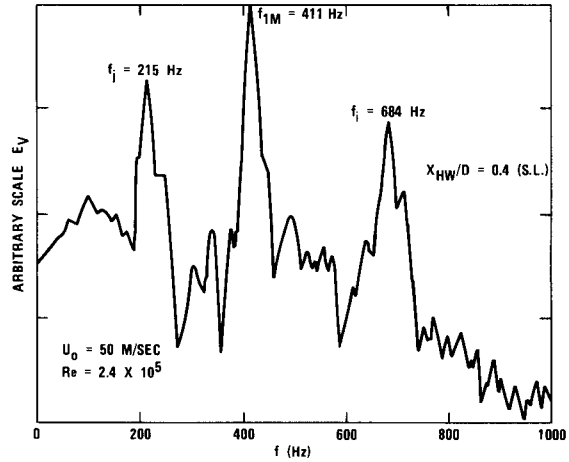

Fig. 2 Unforced flow instability frequencies in initial shear layer.

A similar type of shear layer evolution (with different frequencies) was observed at the higher free and ducted jet velocities. For example, at the highest velocity (140 m/s) and $X_{HW}/D=0.4$, 1220 Hz was the dominant frequency.[16] This frequency was identified as f_{1M}, which has the highest energy level at this axial station. The variation of f_{1M} with U_0 closely followed the theoretical slope of a turbulent flow ($f\approx u^{1.2}$). Furthermore, the preferred mode Strouhal number St_j varied for a freejet velocity of $50<U_0<140$ m/s between 0.25 and 0.33. The spectrum of the velocity fluctuations in the shear layer close to the jet exit for the *ducted* jet had the same frequency peaks as in the freejet, but the corresponding energy level distribution across the shear layer was different.[16]

Effect of Forcing

Both the free and the ducted jets were forced at the instability frequencies f_{1M} and f_j described in the previous section. The jet response to these frequencies was also compared to excitation at an intermediate frequency. Since the main features of the coherent structures dynamics are independent of the viscous effects (or Reynolds number), flow visualization was used in a low-velocity water jet to gain additional understanding of the flow. The unforced ducted flow (Fig. 4a) was compared to the flow characteristics with

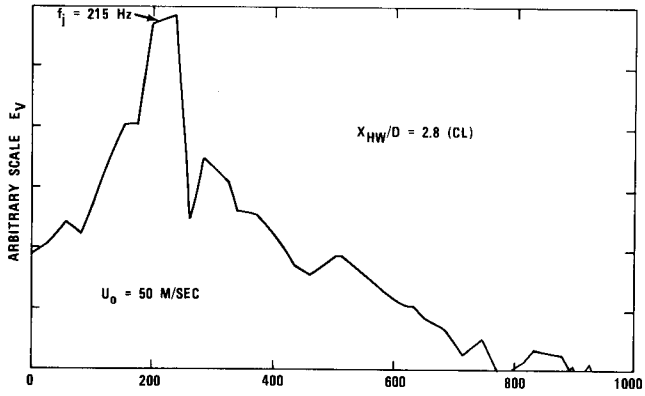

Fig. 3 Preferred mode frequency.

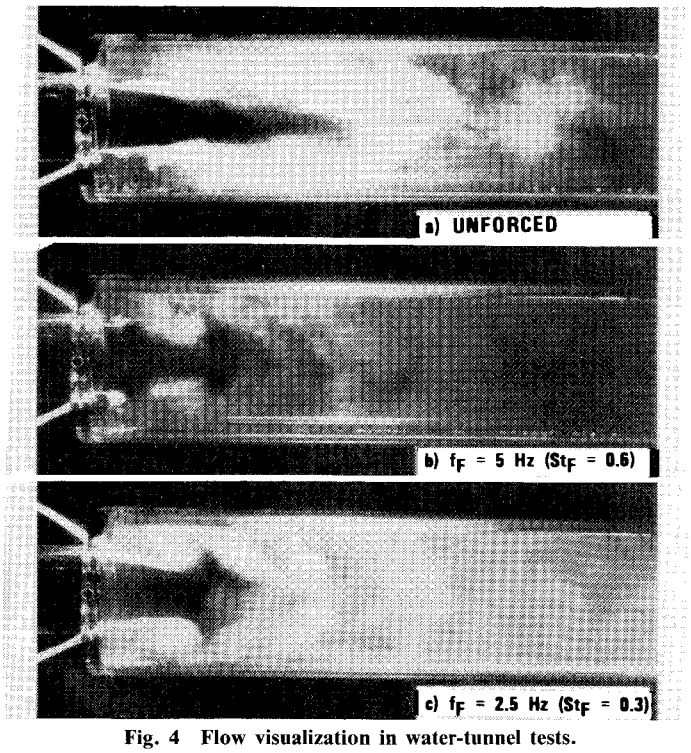

Fig. 4 Flow visualization in water-tunnel tests.

excitations at both the first subharmonic with $f_F = f_{1M} = 5$ Hz (Fig. 4b) and at the preferred mode frequency with $f_F = f_j = 2.5$ Hz (Fig. 4c). The following features of the flow visualization should be emphasized. The initial undisturbed potential core length of the jet was about four nozzle diameters. The initial shear layer and its growth are clearly visible in the unforced case. The potential core length was reduced to about half of its original length when the flow was forced, indicating enhanced mixing. As a result, the shear layer width was increased by forcing the flow. The forcing at the preferred mode frequency had the strongest effect. The flow visualization also showed that the shear layer rolled into large, coherent vortices with forcing at the preferred mode frequency. Forcing at the first subharmonic frequency resulted in smaller coherent structures.

Hot-wire measurements in the airflow tests confirmed the water flow observations. In the airflow experiments, the flow was forced at the first subharmonic with $f_F = f_{1M} = 460$ Hz and at the preferred mode frequency with $f_F = f_j = 230$ Hz. The additional forcing frequency, which did not match any of the instability frequencies, was 300 Hz.

The effect of forcing at different frequencies and amplitudes will be presented for three different flow regimes: the initial shear layer ($X_{HW}/D = 0.4$), the end of the potential core ($X_{HW}/D = 2$), and the pipe flow ($X_{HW}/D > 3.2$). The relative acoustic pressure distribution in the acoustic cavity was determined for each of the nominal forcing frequencies $f_F = 230$, 300, and 460 Hz. The experimental results were in good agreement with simple first longitudinal mode calculations. Figure 5 shows, for example, the comparison between the experimental results and the theoretical calculations for $f_F = 300$ Hz. Figure 5 also shows the spectrum for the pressure transducer located near the dump plane; the highest relative pressure amplitude A_p is approximately 300 Hz. Pressure spectra were computed for each of the forced-jet tests. In the following section, the velocity spectra will be discussed for the different forcing amplitudes and frequencies. Corresponding pressure spectra are described in Ref. 16.

At the forcing frequency of $f_F = 460$ Hz and the amplitude $(\Delta p)_{rms}/P = 0.05\%$, the initial shear layer responded to the forcing frequency, exhibiting a significant peak in the velocity fluctuation energy at that frequency [curve $X_{HW}/D = 0.4$ (*S.L.*) in Fig. 6]. However, no significant peak in the velocity fluctuation spectrum could be identified under the same conditions farther downstream [curve $X_{HW}/D = 2.0$ (*CL*) in Fig. 6]. This can be attributed to the higher amplification of the 460 Hz frequency in the initial shear layer position, where $f_{1M} = 411$ Hz was identified as the most energetic frequency in the unforced jet tests. The fast Fourier transforms (FFT) of the chamber pressure in these tests showed the highest pressure amplitude at 460 Hz. It is interesting to note that forcing the jet by 460 Hz at $X_{HW}/D = 0.4$ changed the spectral distribution of the unforced flow by suppressing the other peaks.

The high peak of the velocity fluctuation energy E_V at 460 Hz in Fig. 6 indicates that, as the result of acoustic forcing, coherent flow structures were generated. The peak energy level compared to the turbulent background level is an indication of the degree of flow coherence.

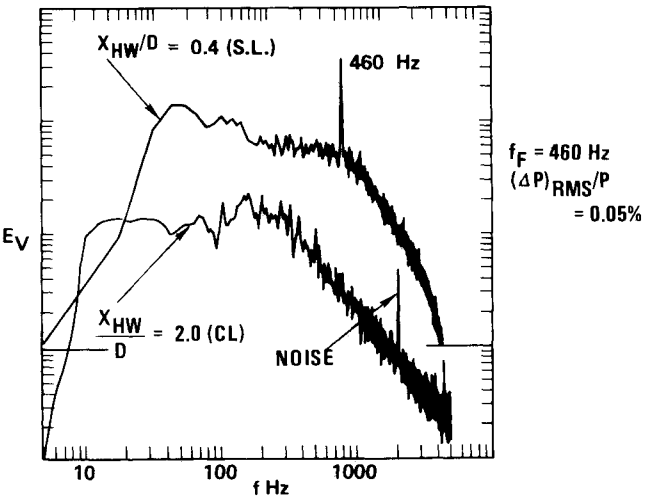

Fig. 6 Response of the flow to low-amplitude forcing.

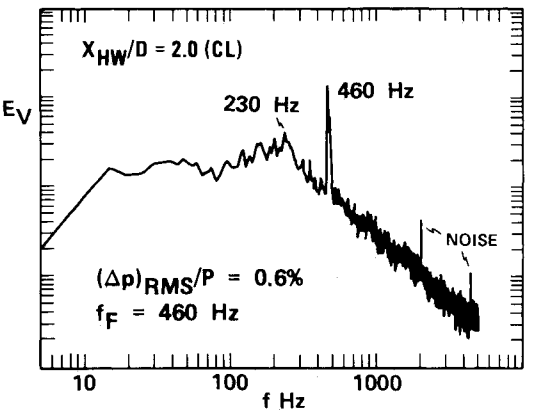

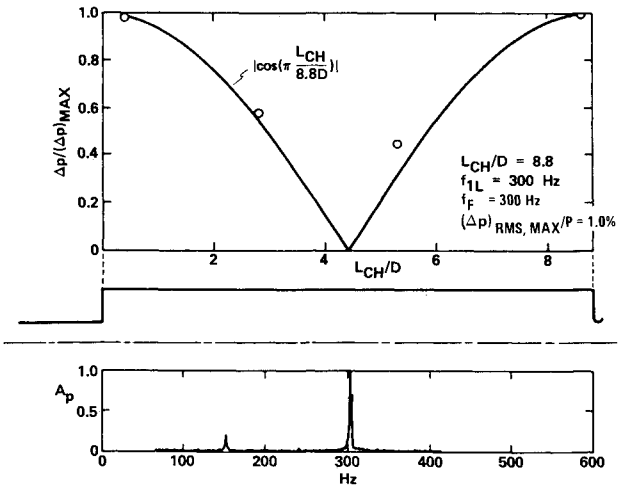

Fig. 5 Acoustic pressure amplitude distribution and spectrum.

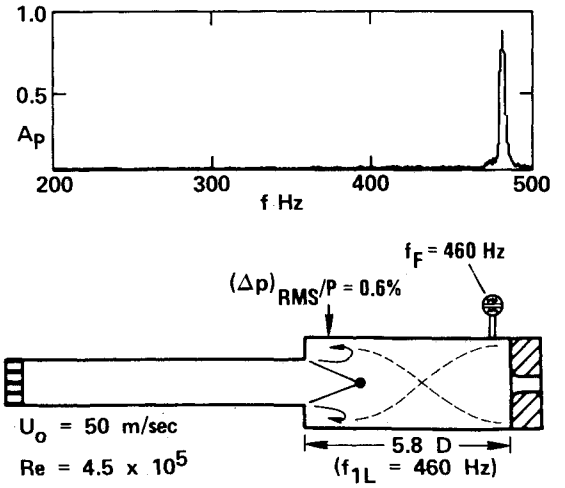

Fig. 7 Velocity spectrum at the end of potential core.

When the forcing level at $f_F = 460$ Hz was increased to $(\Delta p)_{rms}/P = 0.6\%$, the flow responded even at $X_{HW}/D = 2.0$, which is near the end of the potential core where $f_j = 215$ Hz was identified as the unforced, most energetic frequency (Fig. 7). In addition to the energy peak at $f_F = 460$ Hz, a second, broader peak can be identified near 230 Hz, which corresponds to the preferred mode frequency. The energy level E_V at $f_F = 460$ Hz was about three times higher than the turbulent background peak at 230 Hz in this test with $f_F \neq f_j$. This E_V ratio (or the coherence of the flow near the end of the potential core) significantly increased when f_F nearly matched f_j at $X_{HW}/D = 2.0$ (CL). With $f_F = 230$ Hz and the pressure amplitude $(\Delta p)_{rms}/P = 0.16\%$, the velocity fluctuation spectrum had only one peak at 230 Hz. Furthermore, the E_V of the forcing frequency was about eight times higher than the turbulent background level, although the forcing amplitude was significantly less than in the previously discussed test with $f_F \neq f_j$ (Fig. 7). This observation indicates that, at a certain position in the shear layer, the highest amplification of the velocity fluctuations can be achieved when the forcing frequency matches the most energetic local shear layer instability frequency.

For the same forcing amplitude and frequency, namely $(\Delta p)_{rms}/P = 0.16\%$ and $f_F = 230$ Hz, the initial shear layer did not respond to the forcing. At this position, f_F (230 Hz) was about one-half of the most energetic local unforced instability frequency (411 Hz) in the unforced case.

Two tests were made at $f_F \approx 300$ Hz, a frequency that did not match any instability frequency identified in the unforced jet tests. The initial shear layer ($X_{HW}/D = 0.4$) responded insignificantly to the forcing, although the forcing amplitude, $(\Delta p)_{rms}/P = 1.0\%$, was higher than in all the other tests. The flow near the end of the potential core ($X_{HW}/D = 2.0$) did respond. However, the E_V of f_F was only about three times higher than the turbulent background level. In comparison, when f_F and f_j were matched, a lower forcing level of $(\Delta p)_{rms}/P = 0.16\%$ produced an E_V eight times higher at f_F than at the background level.

The effect of forcing the flow at two frequencies was tested by matching f_F to the second acoustic mode, $f_{2L} = 460$ Hz. The FFT's of the pressure showed that for this driving condition the first and second acoustic modes were excited with the relative pressure amplitude A_p of f_{1L} about 5.4 times higher than that of f_{2L}. The pressure wave structure can be considered as a superposition of the first and second acoustic modes as indicated in Fig. 8a. For this driving condition, the highest response (of all the tests) of the jet flow to the acoustic wave was achieved, although the forcing amplitude was at its lowest level with $(\Delta p)_{rms}/P = 0.05\%$. Specifically, the E_V of $f_F/2 = 230$ Hz was about 15 times higher than the turbulent background level near the end of the potential core at $X_{HW}/D = 2.0$ (Fig. 8b). This result might be attributed to a subharmonic resonance mechanism that fed energy into the lower subharmonics when nondispersive flow conditions were obtained.

Temporal cross correlations, also measured in the initial shear layer, revealed a coherent and periodic flow for the 460 Hz forcing at $(\Delta p)_{rms}/P = 0.6\%$. A different behavior showing no periodicity was observed for $f_F = 230$ Hz and $(\Delta p)_{rms}/P = 0.78\%$ at the same cross section.

Additional evidence concerning the different response of the initial shear layer to the two forcing frequencies was obtained by determining the azimuthal spatial cross correlations. These correlations were made at a constant radial distance from the centerline, corresponding to the jet's half-

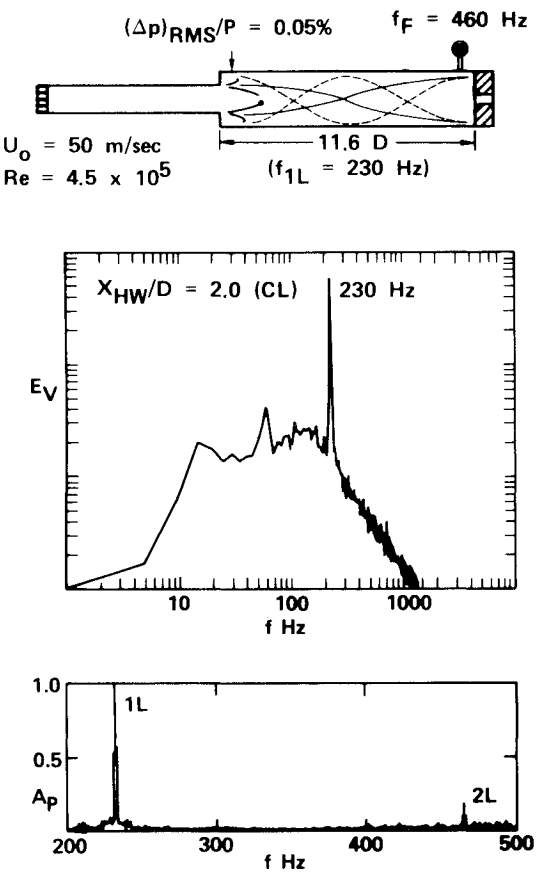

Fig. 8 Velocity spectrum at the end of potential core, when the acoustic forcing was at two subharmonic flow instability frequencies.

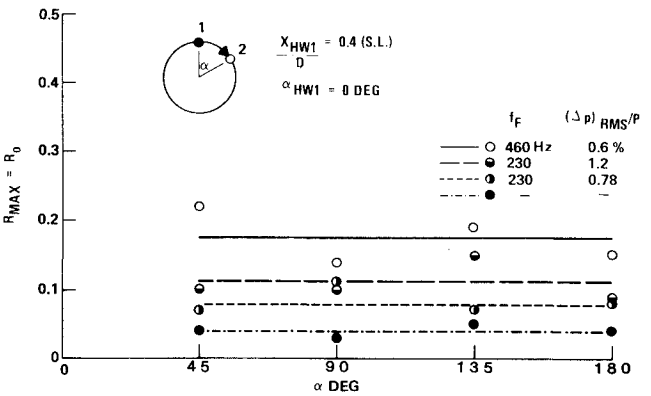

Fig. 9 Azimuthal spatial cross correlation in initial shear layer.

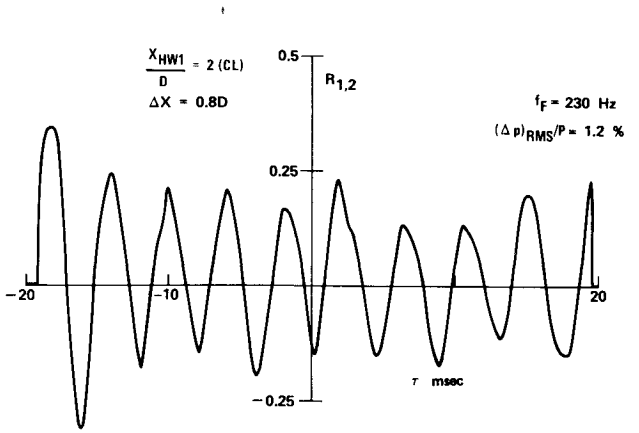

Fig. 10 Temporal cross correlation near end of potential core—high forcing amplitude.

width ($R_{U/U_0=0.5}$) at $X_{HW}/D=0.4$ with varying angle α between the two hot wires (Fig. 9). These measurements provide additional quantitative data on the coherence of the flow structures. As shown in Fig. 9, the highest correlation level was obtained for $f_F=460$ Hz and $(\Delta p)_{rms}/P=0.6\%$. The correlation coefficient at this forcing was of an order of magnitude higher than that of an unforced case. Forcing at $f_F=230$ Hz did not reach the same correlation level, even for the double forcing amplitude of 1.2%. It is also demonstrated in this figure that the coherence indicated by the azimuthal correlations was proportional to the forcing amplitude at $f_F=230$ Hz. The axial convection velocities of the flow structures were determined from the temporal cross correlations at different axial positions in the flow. The values measured were between 0.5 and 0.7 of the initial mean velocity U_0.

Near the end of the potential core, the most energetic frequency was the jet preferred mode. Matching the duct length and the forcing to this frequency resulted in the strongest effect of the forcing on the flow at this regime. Temporal cross correlations made with the first hot wire located at $X_{HW}/D=2$ and the second located at $\Delta X/D=0.8D$ further downstream showed a highly periodic flow when the flow was forced by $(\Delta p)_{rms}/P=1.2\%$ (Fig. 10). Spatial longitudinal cross correlations were also measured at this axial position at different forcing amplitudes (Fig. 11). At the highest forcing amplitude (1.2%), a trend of spatial periodicity can be noticed (broken line). This figure also shows a tendency of the spatial coherence to increase with the forcing amplitude.

Further downstream in the pipe flow regime, the coherence of the flow structures was reduced and the temporal macroscales increased under the preferred mode forcing. This was observed at both forcing amplitudes of 1.2 and 0.78% (Fig. 12).

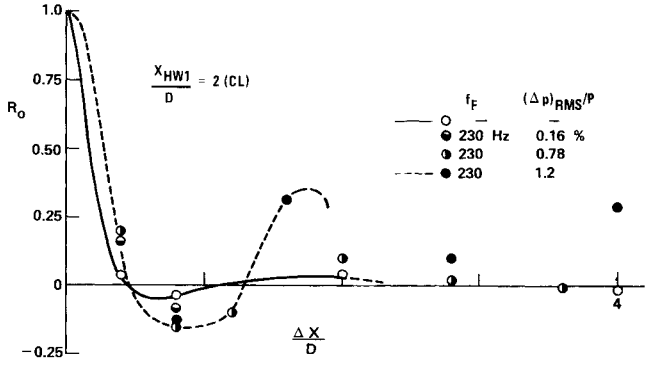

Fig. 11 Longitudinal spatial cross correlation.

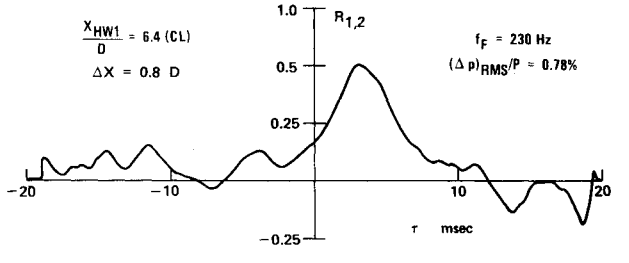

Fig. 12 Temporal cross correlation in pipe flow—low forcing amplitude.

Mean Flow

The acoustically matched preferred mode forcing ($f_F=f_j=$ 230 Hz) with $(\Delta p)_{rms}/P=1.7\%$ had a substantial influence on the mean flow characteristics, except at the jet exit ($X_{HW}/D\approx 0$). At this location, the forced and unforced profiles were almost identical. Further downstream, the spreading rate of the flow was augmented. The normalized mean velocity U/U_0 and the axial turbulence intensity profile u'/U at $X_{HW}/D=1.6$ are shown in Fig. 13. The mean velocity and turbulence increases under forcing. The increase of the mean velocity occurred in the outer side of the shear layer for $R/D>0.3$. This larger jet width resulted in a reduced recirculation zone at the dump, and the reattachment region moved in the upstream direction. The jet core length was also diminished considerably. The intensity of the turbulent axial fluctuations was augmented inside the jet core, $R/D<0.4$ (Fig. 13). This enhanced intensity at the duct centerline reflects a higher spread of the shear layer into the potential core, also yielding the previously mentioned reduction of the core length. The measurements in this figure are given up to the edge of the recirculation zone.

The mean velocity distribution was affected by the preferred mode forcing even further downstream. At $X_{HW}/D=7.2$ (Fig. 14), the mean velocity profile was more evenly distributed for the forced flow than for an unforced flow. This fact demonstrates that by manipulating the flow in the

Table 1 Test conditions[a]

No.	L_{CH}/D	f_F, Hz	$D^2_{t,RV}/D^2_{t,CH}$	$(\Delta p)_{rms}/P$
1	5.8	460	0.09	0.05
2	5.8	460	0.27	0.60
3	11.6	230	0.18	0.78
4	11.6	230	0.27	1.20
5	11.6	230	0.51	1.70
6	8.8	300	0.09	1.00

[a] $D=6.35$ cm, $D_{CH}=2D$, $P=186$ kPa.

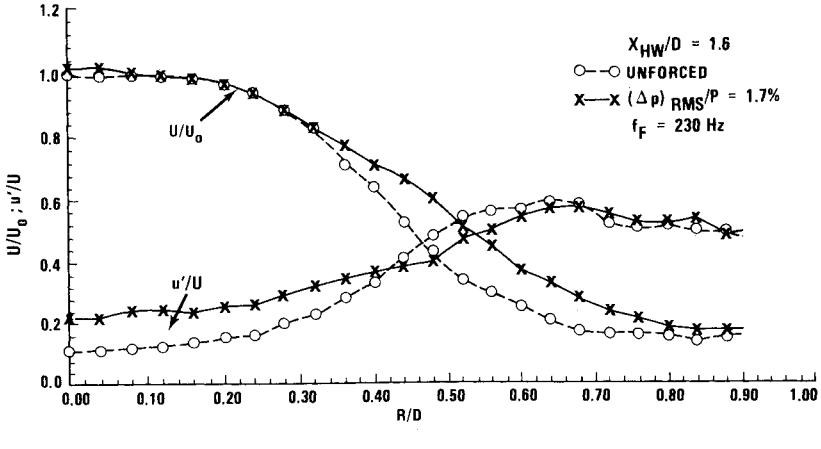

Fig. 13 Unforced and forced radial mean and turbulent velocity profiles across the jet shear layer.

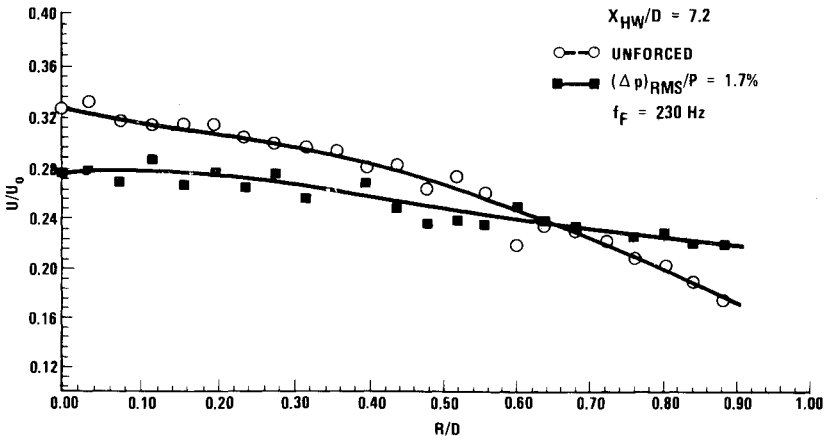

Fig. 14 Unforced and forced radial mean and turbulent velocity profiles in the pipe flow regime.

initial region, the mixing could be enhanced beyond the reattachment zone and into the pipe flow regime.

Conclusions

The results presented in the paper lead to the following conclusions:

1) Large-scale flow structures were identified in the unforced jet with and without duct, even in the highest velocities tested and with turbulent initial conditions.

2) The frequency peaks in the velocity fluctuation spectrum were identified as the most amplified frequency (initial vortex shedding frequency), first vortex merging frequency, and preferred mode frequency. Strouhal numbers for these frequencies were in the range found in previous investigations.

3) In the forced jet tests, the first longitudinal acoustic pressure mode was excited at various forcing amplitudes and frequencies. The highest response of the jet flow to the acoustic waves was obtained when the forcing frequency matched the local most energetic frequency, e.g., with the first vortex merging frequency in the initial shear layer or the preferred mode frequency at the end of the potential core.

4) Under proper forcing conditions, the energy of the velocity fluctuations in the forcing frequency was up to 15 times higher than the turbulent background level. This indicates that highly coherent, large-scale structures were generated even at high Reynolds numbers and forcing amplitudes of less than 1% of the mean chamber pressure.

5) The coherent structures had relatively high azimuthal coherence and were periodic in time and space. Their convection velocity was about 60% of the mean flow velocity.

6) By forcing the flow at the preferred mode frequency, the mixing of the shear layer with both the surrounding recirculation zone and the inside core was enhanced. The recirculation zone and the core were consequently reduced in size.

7) Despite the fact that the coherence of the flow structures was reduced downstream of the core, the enhanced mixing extended past the reattachment zone into the pipe flow regime of the duct.

Acknowledgments

This work was supported by the Office of Naval Research. The authors express their appreciation to Dr. Donna M. Hanson-Parr, Mr. Fred S. Blomshield, and Mr. Jeff B. Foster for their assistance in the analysis of the test data. Thanks are also extended to Rhonda Adair for typing the paper.

References

[1]Brown, G. L. and Roshko, A., "On Density Effects and Large Structures in Turbulent Mixing Layers," *Journal of Fluid Mechanics*, Vol. 64, Pt. 4, 1974, pp. 775–816.

[2]Moore, C. J., "The Role of Shear Layer Instability Waves in Jet Exhaust Noise," *Journal of Fluid Mechanics*, Vol. 80, Pt. 2, 1977, pp. 321–367.

[3]Bechert, D. W., "Sound Absorption Caused by Vorticity Shedding Demonstrated with a Jet Flow," *Journal of Sound and Vibrations*, Vol. 70, Pt. 3, 1980, pp. 389–405.

[4]Tam, C.K.W. and Morris, P. J., "Tone Excited Jets, Part V: A Theoretical Model and Comparison with Experiment," *Journal of Sound and Vibration*, Vol. 102, Pt. 1, 1985, pp. 119–151.

[5]Dunlap, R. and Brown, R. S., "Exploratory Experiments on Acoustic Oscillations Driven by Periodic Vortex Shedding," *AIAA Journal*, Vol. 19, March 1981, pp. 408–409.

[6]Byrne, R. W., AIAA Paper 83-2018, 1983.

[7]Schadow, K. C. et al., "Combustion Instabilities in Liquid Fuel Ramjets," presented at 6th International Symposium on Air Breathing Engines, Paris, 1983.

[8]Crow, S. C. and Champagne, F. H., "Orderly Structure in Jet Turbulence," *Journal of Fluid Mechanics*, Vol. 48, Pt. 3, 1971, pp. 547–591.

[9]Kibens, V., "Discrete Noise Spectrum Generated by an Acoustically Excited Jet," *AIAA Journal*, Vol. 18, April 1980, pp. 434–441.

[10]Michalke, A., "On Spatially Growing Disturbance in an Inviscid Shear Layer," *Journal of Fluid Mechanics*, Vol. 23, Pt. 3, 1965, pp. 521–544.

[11]Winant, C. D. and Browand, F. K., "Vortex Pairing—the Mechanism of Turbulent Mixing Layer Growth at Moderate Reynolds Number," *Journal of Fluid Mechanics*, Vol. 63, Pt. 2, 1974, pp. 237–255.

[12]Ho, C. M. and Huerre, P., "Perturbed Free Shear Layers," *Annual Review of Fluid Mechanics*, Vol. 16, 1986, pp. 365–424.

[13]Wygnanski, I. and Peterson, R. A., "Coherent Motion in Excited Free Shear Flows," AIAA Paper 85-0539, 1985.

[14]Ho, C. M. and Huang, L. S., "Subharmonics and Vortex Merging in Mixing Layers," *Journal of Fluid Mechanics*, Vol. 119, 1982, pp. 443–473.

[15]Gutmark, E. and Ho, C. M., "On the Preferred Modes and Spreading Rates of Jets," *The Physics of Fluids*, Vol. 26, Oct. 1983, pp. 2932–2938.

[16]Schadow, K. C., Wilson, K. J., Crump, J. E., Foster, J. B., and Gutmark, E., "Interaction Between Acoustics and Subsonic Ducted Flow with Dump," AIAA Paper 84-0530, Jan. 1984.

[17]Cohen, J., "Instabilities in Turbulent Free Shear Flows," Ph.D. Thesis, Dept. of Aerospace and Mechanical Engineering, University of Arizona, Tucson, AZ, 1986.